First observation of mechanochromism at the nanometer scale

R.W. Carpick[1], D.Y. Sasaki[2], and A.R. Burns[1,3]

[1] *Sandia National Laboratories, Surface and Interface Sciences, Albuquerque, NM 87185-1413.*

[2] *Sandia National Laboratories, Organic Materials Aging and Reliability, Albuquerque, NM 87185-1407.*

[3] *Corresponding author. E-mail: aburns@sandia.gov, tel: 505-844-9642, fax: 505-844-5470*

Abstract

A mechanically-induced color transition ("mechanochromism") in polydiacetylene thin films has been generated at the nanometer scale using the tips of two different scanning probe microscopes. A blue-to-red chromatic transition in polydiacetylene molecular trilayer films, polymerized from 10,12-pentacosadiynoic acid (poly-PCDA), was found to result from shear forces acting between the tip and the poly-PCDA molecules, as independently observed with near-field scanning optical microscopy and atomic force microscopy (AFM). Red domains were identified by a fluorescence emission signature. Transformed regions as small as 30 nm in width were observed with AFM. The irreversibly transformed domains preferentially grow along the polymer backbone direction. Significant rearrangement of poly-PCDA bilayer segments is observed by AFM in transformed regions. The removal of these segments appears to be a characteristic feature of the transition. To our knowledge, this is the first observation of nanometer-scale mechanochromism in any material.

Introduction

The ability of certain organic molecules to form densely-packed and even self-organized films at surfaces and interfaces provides systems whose chemical, structural, and mechanical properties can be controlled for specific applications. For example, functionalized organic thin films can produce optical responses to specific molecular recognition events, thus providing

DISCLAIMER

molecular sensing capabilities[1]. The optical response of these films is often due to molecular rearrangements or stresses on the chromophoric element. A detailed understanding of the response of such molecules to applied stresses is necessary for further development of these unique sensing materials. Although scanning probe microscope (SPM) probes have been previously used to examine the structure of a wide variety of organic films, we will discuss the first effort to induce color changes in an organic film with SPM probes.

The family of polydiacetylenes (PDAs) is of particular interest as these molecules exhibit strong optical absorption and fluorescence properties that can dramatically change with applied stress (*mechanochromism*)[2-4]. PDAs exhibit chromatic transitions in response to other stimuli, including heat (*thermochromism*)[5,6], changes in chemical environment such as pH[7], and binding of specific biological targets (*affinochromism/biochromism*)[1,8,9]. In general, the observed transition involves a significant shift in absorption from low to high energy bands of the visible spectrum, thus the PDA appears to transform from a blue to a red color. In addition, the red form is highly fluorescent, while the blue form is not. As will be shown here, fluorescence intensity is thus a sensitive gauge of the color transition. The reversibility of the blue-to-red color transition has been observed to depend upon the specific PDA structure and the environmental stimulus. The color transition, along with other properties, such as strong third-order nonlinear susceptibility[10] and unique photo-conduction properties[11], all attributed to the conjugated PDA backbone (Fig. 1), have generated substantially wide interest in PDAs.

Mechanochromism has only been observed in a few instances at macroscopic scales. Müller and Eckhardt observed an irreversible transition in a PDA single crystal induced by compressive stress[2], which resulted in coexisting blue and red phases. Nallicheri and Rubner[3] observed reversible mechanochromism for conjugated PDA chains embedded in a host elastomer that was subjected to tensile strain. Tomioka *et al.* induced reversible chromism by varying the lateral surface pressure of a PDA monolayer on the surface of water in a Langmuir-Blodgett trough[4], with the red form present at higher (compressive) surface pressures. These macroscopic studies of mechanochromism have so far not examined molecular-level structural changes associated with the observed transitions.

The present experiments were conducted using the PDA formed from 10,12-pentacosadiynoic acid (PCDA) monomers (Fig. 1). Topochemical polymerization of the monomers was accomplished through exposure to UV irradiation and required the monomers to

be organized prior to polymerization[12]. Optical absorption occurs within the linear π-conjugated polymer backbone, which hosts delocalized electronic states. The exact mechanism(s) driving the various chromatic transitions are not fully understood. In general, it is believed that molecular conformational changes, such as side chain ordering and orientation, impart stresses that lead to different backbone configurations, thus changing the electronic states and the corresponding optical absorption[6,13]. It is also not established whether the blue-to-red transition is a continuous transition, or a discreet transition between two states separated by an energy barrier. The factors governing the degree of reversibility of the transition are also not understood.

To better understand these chromatic transitions in general, and mechanochromism in particular, we have undertaken scanning probe microscopy (SPM) studies of polymerized PCDA thin films. A SPM tip can be thought of as both an imaging probe and a localized stress actuator. With the appropriate tip structure and using low applied loads, the SPM tip forms a nanometer-scale single asperity contact point with a flat sample[14]. Depending on the specific SPM instrument (as described below), the tip can be used to measure the sample's topographic, frictional, and/or optical responses. For example, an near field scanning optical microscopy (NSOM) probe has been recently utilized by Robinson *et al.*[15] as both an actuator and a spectroscopic tool to observe strain-induced optical emission shifts of quantum dot structures. Using these tools with PDA samples, we have obtained the first observation of mechanochromism at the nanometer scale.

Experimental Section

The details of our sample preparation will be described elsewhere[16]. A brief summary is given here. Both blue and red poly-PCDA films were prepared on a Langmuir trough (Nima, Coventry, UK), that was situated on a vibration isolation table inside a class 100 clean room. The subphase was deionized water with a resistivity greater than 18 MΩ-cm (Barnstead Nanopure system, Dubuque, IA) held at a temperature of 15±1°C. Freshly cleaved muscovite mica substrates were immersed into the subphase prior to monolayer spreading. PCDA molecules (Farchan/GFS Chemicals, Powell, OH), which had been purified through a silica gel column, were spread onto the subphase in a 50% chloroform/benzene solution. On the pure water subphase the monolayer was unstable. Further compression, however, lead to the formation of the stable trilayer. The monomer was compressed at a rate of 50 cm^2/min to a pressure of 20

mN/m, producing a molecular area of ~8 $Å^2$, corresponding to a trilayer configuration[16,17]. The Y-type configuration of these amphiphilic molecules results in the outermost surface layer consisting of hydrophobic methyl-terminated alkyl chains, as shown in Fig. 2. All films were equilibrated for 20 min. at 20 mN/m, prior to UV light exposure (254 nm) with a pair of Hg pen lamps (Oriel, Stratford, CT). Distinct methods were then used to form either blue or red samples, as they exhibited different degrees of rigidity which will be discussed in detail elsewhere[16]. For the blue film: the mica substrate was seated horizontally approximately 1 mm below the water surface before spreading the molecules. The pen lamps, fixed 10 cm from the water surface, were switched on for 30 seconds producing a faintly visible, uniform blue film. The water level was lowered by slowly draining the trough, allowing the polymerized blue film to drape itself over the mica substrate. Vertical transfer was not possible for the blue film as it possessed significant rigidity which prevented film compression during vertical transfer attempts. For the red film: the mica substrate was held vertically below the water surface before spreading the molecules. The monomer film was exposed for 5 minutes with the UV lamps 5.5 cm above the water surface, producing a uniform red film, with a subtle textured appearance. We attribute the textured appearance to the presence of microscopic cracks in the film, as discussed further below. In contrast with the blue film, the cracks presumably allow compressibility of the red film during vertical transfer. The film was transferred to the mica substrate by drawing it upward at a rate of 10 cm/sec while holding the trough pressure constant. Both samples were dried in clean room air and stored in a dark, nitrogen-purged container.

Samples were analyzed with several techniques. Microscopic (far-field) sample fluorescence was recorded using a Leitz optical fluorescence microscope equipped with dichroic beam filters and polarized white light from a Xenon lamp. A CCD camera was used to capture the field of view for the images presented here. An atomic force microscope (AFM) (Nanoscope IIIA, Digital Instruments, Santa Barbara, CA) operating in contact mode with silicon nitride cantilevers was used to obtain topographic and friction force images. Measurements with the AFM were acquired under laboratory ambient conditions. The scan rate was 3 Hz (= lines/sec) unless otherwise noted.

A home-built NSOM integrated with an interfacial force microscope (IFM) sensor was used to obtain simultaneous optical, shear force and normal force measurements at the nanometer scale (Fig. 3). This instrument is described in more detail elsewhere[18,19]. The IFM is used here to

determine the applied load during scanning, completely decoupled from the shear-force signal. Topographic feedback is accomplished using shear-force damping, as described below. The NSOM operates in reflection mode. Less than 0.5 mW of polarized 488 nm light from an Ar laser is launched into a single-mode fiber optic. The other end of the fiber is tapered by conventional fiber pulling[20] or chemical etching[21], and coated with ~80 nm Al. Scanning electron microscopy imaging confirms the tips are ~100 nm diameter or less. The fiber is mounted onto a small piezo-electric transducer that oscillates the fiber laterally. The fiber typically has a mechanical resonance at 25-50 kHz, depending on the free length (typically ~3mm), a typical Q-factor of 100 (before contact) and a free lateral motion amplitude of typically 9 nm. Detection of fiber motion is accomplished non-optically by monitoring induced voltages on the drive piezo[22]. The tip is brought close to the sample using a stepper motor. Final approach and topographic distance control is accomplished by a second piezo tube, upon which the sample and IFM force sensor are mounted. The fiber amplitude is attenuated upon interaction of the probe tip with the sample. Topographic images were obtained by rastering the tip across the sample while maintaining constant shear force damping (thus, contrast can occur due to true sample topography or higher friction[19]). A ×36 Schwarzschild objective (NA=0.5) collects sample fluorescence concentric about the tip. Reflected 488 nm light is attenuated with a holographic notch filter, and a 530 nm cutoff filter is used to eliminate signal due to Raman scattering in the fiber. The sample fluorescence is focussed into a spectrometer (ISA/SPEX, Edison, NJ) and the signal is measured with a cooled photomultiplier tube and photon-counting electronics. The entire apparatus in enclosed and continuously purged with N_2 gas to eliminate capillary condensation between the tip and sample. The relative humidity was typically <5% for all experiments.

Sample Characterization

The optical absorption spectra of both the blue and red films are consistent with previously reported spectra[6]. Far-field fluorescence microscopy reveals that the red films are strongly fluorescent and organized into crystalline domains. The fluorescence images show extended cracks in the films that are roughly parallel. In Fig. 4, the excitation light is polarized along the crack direction. The fluorescence emission is almost completely extinguished by rotating the polarization of the excitation light by 90°. Both the absorption and emission dipole of PDA is

known to be aligned along the backbone direction[23-25]. Thus, the domains we observe consist of highly oriented backbones, parallel to the cracks. Topographic AFM images are consistent, showing uniform terraces with roughly aligned cracks (Fig. 5), similar to previous reports[17,26]. The cracks expose the mica substrate, as verified by the higher friction force measured within the cracks. The film height measured at these crack edges is ~9.0±0.9 nm, corresponding to the height of a poly-PCDA trilayer with a nominal ~20° tilt of the molecule (the extended PCDA molecule is ~3.2 nm in length[6,27]). As mentioned previously, a trilayer structure is indicated by the pressure-area isotherms from the Langmuir trough. The tilt angle is similar to previous reports of Cd salts of the same molecule[28]. In addition, islands ~6.1±0.6 nm in height are found on top of the trilayer. The height measurement indicates that the islands consist of an additional bilayer of poly-PCDA with the same tilt angle. The bilayers are likely stabilized by interfacial hydrogen-bonded ad dimers of the acid head groups and thus present methyl groups to the tip as well. Indeed, there is no friction force contrast between the surface of the trilayer or the extra bilayer islands. The bilayers are likely produced during the monomer compression stage before polymerization and deposition.

Blue PCDA samples show only weak fluorescence, where this weak emission appears to be localized at film cracks, edges and other defects. AFM imaging reveals large, uniform terraces, with a few film defects that expose the mica substrate (Fig. 6). The trilayer film height is ~7.4±0.8 nm, ~18% less than the red PCDA trilayer. This indicates that poly-PCDA molecules may be more tilted away from the surface normal in the blue phase (tilt angle ~39°), and additionally the height may be reduced by an altered backbone configuration. This is consistent with poly-PCDA trilayer height measurements of Lio *at al.* [6], where blue PCDA trilayers were 15% shorter than the red phase which was formed thermochromically. X-ray diffraction measurements of poly-PCDA multilayers also indicate the red phase (formed by UV irradiation) is substantially less tilted from the surface normal than the blue[29]. As with the red sample, bilayer islands atop the trilayer base are occasionally observed. High resolution images on the terraces reveal large, extended arrays of parallel striations (see Fig. 10), similar to previous reports[6]. The striations correspond to the backbone direction. This indicates that the backbones are also highly oriented within individual domains in the blue phase.

While the microstructural features of both the blue and red films involve cracks, extra bilayer islands and other defects, we observe with both blue and red films that large, crystalline domains

comprise a significant fraction of the sample. These domains are atomically flat and have a high degree of backbone ordering. We conclude overall that both blue and red film quality within these individual domains is extremely high at the molecular level. From the trilayer configuration of the films, as depicted in Fig. 2, we assert that the acid-mica and acid-acid interfaces are more strongly bound due to hydrogen bonding, while the methyl-methyl interface is less strongly bound.

Results and Discussion

Tip-Induced Mechanochromism. Red PCDA samples were examined with the NSOM/IFM instrument and exhibited fairly uniform fluorescence, with no changes induced by tip-sample contact. Simultaneous shear-force topography and polarization-sensitive fluorescence images are consistent with those previously obtained for red films using transmission-mode NSOMs[24,30]. A typical near-field fluorescence spectrum is shown in Fig. 7. The spectral features, a large peak at ~640 nm and a smaller peak at ~560 nm, are consistent with previous reports of red PDA fluorescence[31]. Note that the 530 nm cutoff filter attenuates the high energy tail.

Blue PCDA samples were investigated with the NSOM/IFM instrument. Fig. 8 shows simultaneous 2.4×2.4 μm^2 shear force topography and fluorescence images, obtained with the monochromator set at 640 nm. The shear force damping was set to a constant value of 15% for a ~9 nm free amplitude. The dither direction is aligned with the vertical axis of the image. In Scan 1, the shear force topography is essentially flat, with identifying defective features on the right side of the image. The fluorescence image shows only an extremely weak and uniform noise background characteristic of blue films (Fig. 9).

Upon imaging the same region a second time, dramatic local changes occur. The arrow in Fig. 8, Scan 2 indicates the polymer backbone direction, as identified by other images within the same poly-PCDA domain which show striations aligned along that direction (the pre-existing defect is also oriented along this direction and may correspond to a step or crack in the film). The shear force topography displays features, of *apparent* high topography, that consist of stripes along the backbone direction. The fluorescence image shows a new localized response coincident with the topographic features. A fluorescence spectrum obtained over this region reveals the spectral fingerprint of red PCDA (Fig. 9). The fluorescence region grows larger with

subsequent imaging. This effect was reproduced multiple times as well as with a separate NSOM tip and a separate blue PCDA sample. In general, when this transition is observed, the fluorescent regions grow gradually with each image acquired. We postulate that the transition takes place during the image acquisition itself, in the case of Fig. 8. The example in Fig. 8 represents one of the largest changes between subsequent images that we observed. Simultaneous normal force measurements with the IFM while under shear-force feedback reveal that this transition can occur with either negative or positive applied loads. The slow imaging speed required to collect NSOM fluorescence images combined with drift of the IFM sensor prevented us from performing a detailed correlation of domain growth rate and normal load at this time. Typically, applied loads were in the range of –20 nN to +20 nN, where the minimum possible load (or "adhesion force") was in the range of –30 nN to –70 nN.

Unfortunately, the spatial resolution of the fluorescence image in Fig. 9 is lower than expected given the ~100 nm tip aperture. This resolution degradation was due to scattering of the exciting 488 nm light in the mica substrate. Mica provides an ideal flat substrate for excellent film quality. Since the film quality was of utmost importance, we therefore settled with less-than-optimal lateral resolution for collection of fluorescence images.

The blue-to-red transition was then investigated with the AFM. For AFM measurements, applied loads were in the range of –20 nN to +10 nN, where the minimum possible load (or "adhesion force") was in the range of –5 nN to –40 nN. The scan speed was 3 μm/sec. Fig. 10 shows excerpts from a series of topographic images (1×1 μm^2) where a distinct region progressively grows due to scanning. Backbone-related striations are seen in the images. The region, initially only 30 nm wide[32], preferentially grows along the backbone direction but also grows, more slowly, perpendicular to the backbone direction. The topographic details of this transformed region are discussed further below. To verify that this was indeed the same transition observed in the NSOM/IFM experiments, a large area was patterned by repeated scanning. Figs. 11a and 11b respectively show the initial and final 10×10 μm^2 topographic images. Several defects, such as film cracks (dark) and extra bilayer islands atop the trilayer (bright) are seen. Fig. 11c shows the same region viewed under the far-field fluorescence microscope. Characteristic red PCDA fluorescence is localized within the patterned region. The fluorescence persists for at least 30 days, indicating that the transition is irreversible.

We have observed that heating blue PCDA samples to ~60°C also causes an irreversible blue-to-red transition (thermochromism)[6]. This raises the possibility that SPM tips are locally heating the PCDA during scanning, thus causing the observed transition[33-35]. However, AFM tips are not actively heated, and the transition occurs for NSOM tips even without the laser excitation present. Local heating arising from friction between the tip and PCDA cannot account for the transition, as phonons excited by tip-sample contacts are in general predicted to rapidly propagate away from the contact zone[36]. In other words, the tip and sample act as large thermal baths for the contact. Significant heating of the contact zone is therefore unfeasible.

Observations of several transitions with both NSOM/IFM and AFM reveal the following properties:

- Although transitions are observed in apparently defect-free regions, defects in the film such as pinholes and crack edges assist significantly in the initial formation and growth of the fluorescent domains of the red form.
- The transition does not proceed without sliding contact occurring between the tip and sample, *i.e.*, *shear forces are required.* The transition is always initiated and grows within the imaging region (where tip-sample sliding contact occurs). Furthermore, the transition will often extend outside the imaging region, indicating that the transition propagates along the backbone direction beyond the region of contact. Engagement of AFM force-distance profiles, where the normal load is varied without allowing lateral motion of the tip, does not contribute to the domain formation or growth.
- As verified with the AFM, the growth proceeds most rapidly when the sliding (fast scan) direction is perpendicular to the backbone chains[37]. In most cases, growth will not proceed at all when the fast scan direction is parallel to the backbone chains.
- Nucleation and growth of the red domains occurs at negative applied loads, but the growth proceeds faster at larger loads. Note that finite shear forces persist even at negative loads in an adhesive contact[18,19,38]. Imaging at very low, negative loads in the absence of significant adhesion effectively provides a method of imaging the sample without promoting further growth.
- The rate of growth varies between samples, and even within a single sample, suggesting that the transition rate is highly dependent on sample preparation conditions (such as UV exposure), local defect density, and the film/substrate interface. This variation makes it difficult to quantify

the exact load dependence of the growth without a large number of further experiments. However, it is clear that shear forces perpendicular to the backbone are required.

Role of Topographic Structural Changes. As mentioned previously, the red PCDA film formed by UV exposure is taller than the blue PCDA film by ~18%. However, the red regions formed by tip-induced mechanochromism generally exhibit *lower* topography, such as in Fig. 10. Substantial corrugation is often observed within these regions as well (Fig. 12a). The depth of the lower regions varies but is frequently observed to be ~4.3±0.3 nm below the trilayer. This suggests that material is removed during the transformation process. Note that a complete crack in the blue trilayer film exposing the mica substrate has a height of ~7.4 nm, thus the film has not been completely removed from this region. Indeed, high resolution images within these lower regions reveal the familiar backbone-related structure, verifying that poly-PCDA remains (Fig. 12a). However, the removal of a bilayer of blue PCDA (layers 2 and 3, Fig. 2) should produce a depth of 4.9 nm. If we assume that the remaining monolayer (layer 1, Fig. 2) has been converted to the red form, and possesses 1/3 of the height of the red trilayer formed by UV polymerization, then a depth of 4.3 nm is expected (see Fig. 13a), consistent with the observed depth. Also, within these regions, strands with height ~2.3 – 2.9 nm are frequently observed, and are correlated with higher friction, suggesting that these features are COOH-terminated monolayer strands.

These AFM measurements at first appear to contradict the NSOM shear-force topography image in Fig. 8, where the transformed region appears *higher* than the surroundings. However, topographic contrast reversal has been previously reported for other materials examined with NSOM[39], as the shear force topography mode is highly sensitive to friction forces and structural effects. With our samples, highly corrugated regions with exposed COOH-terminated strands will produce higher friction than CH_3-terminated strands, as could other defects in the region, thus leading to regions of higher *apparent* topography. This has been recently observed in a comparison between CH_3 and COOH-terminated thiol films[18,19]. This effect will depend on the amount of COOH-terminated strands present, as well as the applied load, and the NSOM tip structure and composition. Indeed, we have observed other transformed regions with NSOM that possess apparent *lower* topography. We propose that the NSOM and AFM transitions produce essentially the same topographic structural changes despite the differences in *apparent*

topography, and we refrain from using the apparent topography in NSOM shear force images as an indication of true topography.

As mentioned above, certain observations of the transition induced with AFM produced regions with significant corrugation (Fig. 12). The highest points of the transformed region are quite variable, but are typically 4.5 – 5.5 nm higher than the surrounding trilayer, roughly consistent with the height of a PCDA bilayer segment. The observed heights of these features are too variable to classify them as either the blue or red form by virtue of their height. Note that in Fig. 11b it is apparent that a bilayer island has grown significantly in size after the scanning procedure. Therefore, significant rearrangement of PCDA bilayer segments occurs during the transformation, and occasionally monolayer segments with exposed acid groups are created as well.

From these results, we can propose three distinct processes for the mechanically-induced transition:

(1) Shear forces between the tip and sample displace segments of the topmost bilayer (layers 2 and 3, Fig. 2). The underlying monolayer (layer 1, Fig. 2) then adopts the red configuration (Fig. 13a) as a result of its altered environment (with no molecules above it any longer), or by the subsequent application of shear forces during scanning.

(2) Shear forces between the tip and sample break polydiacetylene backbone bonds, producing oligomers with shorter backbone lengths within the upper layers. The shorter backbone length allows the oligomers to adopt the red configuration (Fig. 13b).

(3) Shear forces between the tip and sample directly distort the molecular conformation from the blue to the red state. The rearrangement of bilayer segments is an independent side-effect. In other words, all or most of the molecules in the affected region adopt the red configuration (Fig. 13c).

The first process is consistent with our observations, particularly the measured height differences between the monolayer and the surrounding blue trilayer with AFM. It is also consistent with the observation that step edges and pinhole defects in the film assist in the transition, as such vacancies allow the instigation of molecular displacement via lateral motion. This displacement would obviously be significantly restricted in a defect-free region. The second process seems unlikely for several reasons. First, isolated bilayer islands observed on blue samples, being limited in size, clearly consist of oligomers with shorter backbone lengths than

the complete trilayer below, yet these islands are not observed to be fluorescent. Second, it would not explain why layer 1 appears to possess the height of red PCDA after the transition has occurred. Finally, some observations of the transition do not appear to produce such bilayer segments in any uniform fashion (e.g. Fig. 10, Fig. 11); the newly-formed red regions mostly possess lower topography. The third process is not supported by the consistently-observed correlation between molecular displacement and the blue to red transition, nor does it explain the observed height of layer 1. Therefore, the first process appears to occur in this system. How the remaining monolayer is converted to the red form remains to be explained and is discussed below.

It has been suggested that the red phase involves alkyl side chain entanglement and disorder [40,41]. However, recent evidence suggests otherwise. AFM images that resolved the atomic lattice of blue and red PCDA trilayers were obtained by Lio *et al.* They observed that the red phase, formed thermochromically, displayed a *higher* degree of ordering of the alkyl side chains. In the red phase, the chains formed a close-packed hexagonal arrangement, whereas in the blue phase, a partially disordered arrangement was observed. Preliminary high-resolution AFM results suggest that our UV-formed red films exist in a highly ordered arrangement. Furthermore, FTIR data of Lio *et al.*[6] and ^{13}C NMR data of Tanaka *et al.*[42] suggest that some of the tilted side chains rotate toward the surface normal in the red phase. Such a rotation is consistent with the observed height increase of the red phase, and would impart stress to the polymer backbone. In particular, it could lead to rotation about the C—C bond of the polymer backbone, thus changing the planarity of the backbone (Fig. 14). Theoretical calculations indicate that a rotation of only 5° about this bond dramatically changes the π-orbital overlap[43] (shown schematically in Fig. 14), causing a significant blue-shift of the absorption spectrum. As suggested by Cheng and Stevens[7], one example of a possible structure that disrupts backbone planarity is a staggered configuration of the side-chains. In general, a combination of C—C bond rotations in the backbone with gauche defects in the side chains could produce blue and red phases with distinct side-chain packing.

In the absence of the alkyl side chains, there would be a monotonic change in the energy of the polymer backbone as the C—C bond angle changes[43,44]. The torsional mobility of the polymer backbone is restricted by alkyl side chain packing and H-bonding of the head groups[44]. The irreversibility of the transition we observe indicates the greater stability of the red phase compared to the blue. The competing factors of backbone stress, side chain orientation and

spacing, and head group H-bonding may lead to two distinct phases separated by an energy barrier – a metastable blue phase, and a more stable red phase. The energy to overcome this barrier could be provided by the tip. The applied shear stress assists in rotating and deforming the methyl-terminated alkyl side chains into the more stable red configuration. Note that this requires the shear force to be applied perpendicular to the polymer backbone; indeed we observe that shear forces perpendicular to the backbone are most efficient in generating the transition. Alternately, the removal of the uppermost bilayer (layers 2 and 3, Fig. 2) may change the stresses acting on the monolayer (layer 1, Fig. 2), thus allowing it to transform to the red phase. We are unable to suggest a mechanism by which this transition occurs in this case. In either event, it would clearly be advantageous to study a stable PDA *monolayer*, to reduce the complications associated with analyzing substantial molecular displacement. Efforts to produce a stable PDA monolayer are underway.

Summary

For the first time, the blue-to-red chromatic transition of a trilayer polydiacetylene thin film has been induced using a nanometer-scale probe tip. Shear forces between the tip and PCDA molecules in the blue phase create nanometer-scale red domains that preferentially nucleate at film defects and propagate along the polymer backbone. The transition is irreversible and appears to be discreet. Significant displacement of the PCDA molecules is observed within the red domains. Removal of the uppermost bilayer appears to be correlated with the transition, where the remaining monolayer exists in the red phase. The transition is reproducibly observed with both AFM and NSOM probe tips. The rate of domain formation increases with applied load and hence with higher shear forces and is favored when shear forces are applied perpendicular to the backbones. The shear force-induced transition is consistent with models that invoke side-chain rotation about the conjugated backbone. Future work will focus on quantifying the shear forces and loads required to cause this transition for both trilayer and monolayer PDA films, as well as molecular dynamics simulations of the molecular conformation in both the blue and red phase. We hope that these efforts will then allow us to precisely correlate molecular conformational changes with color transitions in these fascinating materials.

Supporting Information Available

Two movies of the color transition, each composed of a series of topographic AFM images, can be viewed at <http://www.sandia.gov/surface_science/nsom/nsom.htm> . These movies illustrate very clearly the anisotropic growth of the domains, and the structural changes that accompany the transition.

Acknowledgments

We gratefully acknowledge S. Singh who assisted with PCDA film preparation and analysis and provided useful discussions. We acknowledge useful discussions with D.H. Charych, U. Jonas, J. Houston and T. Michalske. R.W.C. acknowledges the support of the Natural Sciences and Engineering Research Council of Canada. Sandia is a multiprogram laboratory operated by Sandia Corporation, a Lockheed Martin Company, for the United States Department of Energy under Contract DE-AC04-94AL85000.

REFERENCES

(1) Charych, D. H.; Nagy, J. O.; Spevak, W.; Bednarski, M. D. *Science* **1993**, *261*, 585.

(2) Muller, H.; Eckhardt, C. J. *Mol. Cryst. Liq. Cryst.* **1978**, *45*, 313.

(3) Nallicheri, R. A.; Rubner, M. F. *Macromolecules* **1991**, *24*, 517.

(4) Tomioka, Y.; Tanaka, N.; Imazeki, S. *J. Chem. Phys.* **1989**, *91*, 5694.

(5) Wenzel, M.; Atkinson, G. H. *J. Am. Chem. Soc.* **1989**, *111*, 6123.

(6) Lio, A.; Reichert, A.; Ahn, D. J.; Nagy, J. O.; Salmeron, M.; Charych, D. H. *Langmuir* **1997**, *13*, 6524.

(7) Cheng, Q.; Stevens, R. C. *Langmuir* **1998**, *14*, 1974.

(8) Reichert, A.; Nagy, J. O.; Spevak, W.; Charych, D. *J. Am. Chem. Soc.* **1995**, *117*, 829.

(9) Charych, D.; Cheng, Q.; Reichert, A.; Kuziemko, G.; Stroh, M.; Nagy, J. O.; Spevak, W.; Stevens, R. C. *Chemistry & Biology* **1996**, *3*, 113.

(10) Kobayashi, T. *Optoelectronics - Devices and Technologies* **1993**, *8*, 309.

(11) Hoofman, R. J. O. M.; Siebbeles, L. D. A.; de Haas, M. P.; Hummel, A.; Bloor, D. *J. Chem. Phys.* **1998**, *109*, 1885.

(12) Mowery, M. D.; Menzel, H.; Cai, M.; Evans, C. E. *Langmuir* **1998**, *14*, 5594.

(13) Bloor, D.; Chance, R. R. *Polydiacetylenes: Synthesis, Structure, and Electronic Properties*; Martinus Nijhoff: Dordrecht, 1985, pp xvi.

(14) Carpick, R. W.; Salmeron, M. *Chem. Rev.* **1997**, *97*, 1163.

(15) Robinson, H. D.; Muller, M. G.; Goldberg, B. B.; Merz, J. L. *Appl. Phys. Lett.* **1998**, *72*, 2081.

(16) Sasaki, D. Y.; Carpick, R. W.; Burns, A. R. *in preparation* **1999**.

(17) Goettgens, B. M.; Tillmann, R. W.; Radmacher, M.; Gaub, H. E. *Langmuir* **1992**, *8*, 1768.

(18) Burns, A. R.; Houston, J. E.; Carpick, R. W.; Michalske, T. A. *Phys. Rev. Lett.* **1999**, *82*, 1181.

(19) Burns, A. R.; Houston, J. E.; Carpick, R. W.; Michalske, T. A. *Langmuir* **1999**, *15*, 2922.

(20) Betzig, E.; Trautman, J. K.; Harris, T. D.; Weiner, J. S.; Kostelak, R. L. *Science* **1991**, *251*, 1468.

(21) Hoffmann, P.; Dutoit, B.; Salathe, R. P. *Ultramicroscopy* **1995**, *61*, 165.

(22) Barenz, J.; Hollricher, O.; Marti, O. *Rev. Sci. Instrum.* **1996**, *67*, 1912.

(23) Chance, R. R.; Patel, G. N.; Witt, J. D. *J. Chem. Phys.* **1979**, *71*, 206.

(24) Moers, M. H. P.; Gaub, H. E.; Vanhulst, N. F. *Langmuir* **1994**, *10*, 2774.

(25) Yamada, S.; Shimoyama, Y. *Jpn. J. Appl. Phys. 1, Regul. Pap.* **1996**, *35*, 4480.

(26) Putman, C. A. J.; Hansma, H. G.; Gaub, H. E.; Hansma, P. K. *Langmuir* **1992**, *8*, 3014.

(27) J.A. Shelnutt (personal communication).

(28) Lieser, G.; Tieke, B.; Wegner, G. *Thin Solid Films* **1980**, *68*, 77.

(29) Fischetti, R. F.; Filipkowski, M.; Garito, A. F.; Blasie, J. K. *Phys. Rev. B* **1988**, *37*, 4714.

(30) Kramer, A.; Hartmann, T.; Eschrich, R.; Guckenberger, R. *Ultramicroscopy* **1998**, *71*, 123.

(31) Olmsted, J.; Strand, M. *J. Phys. Chem.* **1983**, *87*, 4790.

(32) The 30 nm width is likely limited by the contact area between the tip and sample. A smaller tip may be capable of producing a transformed region even smaller in size.

(33) Kavaldjiev, D. I.; Toledo-Crow, R.; Vaez-Iravani, M. *Appl. Phys. Lett.* **1995**, *67*, 2771.

(34) Stahelin, M.; Bopp, M. A.; Tarrach, G.; Meixner, A. J.; Zschokke-Granacher, I. *Appl. Phys. Lett.* **1996**, *68*, 2603.

(35) La Rosa, A. H.; Yakobson, B. I.; Hallen, H. D. *Appl. Phys. Lett.* **1995**, *67*, 2597.

(36) Perry, M. D.; Harrison, J. A. *J. Phys. Chem.* **1995**, *99*, 9960.

(37) The applied shear forces in NSOM are more complicated than in AFM. Dithering of the fiber exerts oscillatory shear forces at 25-35 kHz during imaging, roughly along the vertical direction of Fig. 8. Rastering of the tip exerts additional shear forces at a few Hz along the "fast-scan" direction, which is the horizontal direction of Fig. 8.

(38) Carpick, R. W.; Agraït, N.; Ogletree, D. F.; Salmeron, M. *J. Vac. Sci. Technol. B* **1996**, *14*, 1289.

(39) Durkan, C.; Shvets, I. V. *J. Appl. Phys.* **1996**, *79*, 1219.

(40) Saito, A.; Urai, Y.; Itoh, K. *Langmuir* **1996**, *12*, 3938.

(41) Mino, N.; Tamura, H.; Ogawa, K. *Langmuir* **1991**, *7*, 2336.

(42) Tanaka, H.; Gomez, M. A.; Tonelli, A. E.; Thakur, M. *Macromolecules* **1989**, *22*, 1208.

(43) Orchard, B. J.; Tripathy, S. K. *Macromolecules* **1986**, *19*, 1844.

(44) Dobrosavljevic, V.; Stratt, R. M. *Phys. Rev. B* **1987**, *35*, 2781.

FIGURE CAPTIONS

Fig. 1(a) Monomeric and (b) polymeric form of PCDA.

Fig. 2. Trilayer packing of PCDA molecules. The circle represent the COOH head groups which are expected to hydrogen bond to the mica substrate (mica-layer 1 interface) and each other (layer 2-layer 3 interface). Between layers 1 and 2 is a CH_3-CH_3 interface that is less strongly bonded through van der Waals forces.

Fig. 3. Schematic diagram of the NSOM/IFM instrument. The NSOM fiber is brought into contact with a sample resting on an IFM sensor. The sensor measures the attractive and repulsive normal forces between the tip and sample by maintaining an electrostatic balance of two capacitances C_1 and C_2, formed by the common plate and identical gold pads fixed on a glass substrate (not shown). Exciting light is launched into the fiber and excites sample fluorescence in the near field. Light is collected in the far-field above the sample by an objective (not shown).

Fig. 4. Fluorescence microscopy images (170×130 μm^2) of fully red PCDA at 0° and 90° polarization relative to the horizontal direction. At 0°, cracks are observed in the trilayer film. At 90°, emission from this single domain is largely extinguished, indicating a high degree of orientation of the polymer backbones.

Fig. 5. Topographic AFM image (50×50 μm^2) of fully red PCDA. The sample shows high coverage, with roughly parallel cracks. The cracks are oriented along the polymer backbone direction.

Fig. 6. Topographic AFM image (50×50 μm^2) of blue PCDA. The sample also shows high coverage, with a few isolated holes in the film.

Fig. 7. Near-field fluorescence spectrum of fully red PCDA, showing characteristic peaks at 640 nm and 560 nm.

Fig. 8. NSOM shear force topography (left) and simultaneous fluorescence (right) images acquired (2.4×2.4 μm^2) showing tip-induced mechanochromism. In the first scan (top), no fluorescence is seen over the flat PCDA region. In the subsequent scan, topographic changes are created, and fluorescence emission is produced within the imaging region. The topographic features display alignment along the polymer backbone direction (arrow).

Fig. 9. Near-field fluorescence spectrum of blue PCDA, before and after tip-induced mechanochromism. Before the transition, only a weak background is observed. The fluorescence spectrum after the transition shows the same characteristic peaks (at 640 nm and 560 nm) as fully red PCDA, formed through UV polymerization.

Fig. 10. Series of 1×1 μm^2 topographic AFM images showing the progressive growth of the tip-induced red domains. In the first scan, striations indicative of the polymer backbone direction are observed. By the fourth scan, a topographically distinct (*i.e.* lower) region, only 30 nm wide, appears. This region continues to grow in subsequent scans.

Fig. 11. Patterning of red PCDA domains. Initial (a) and final (b) 10×10 μm^2 topographic AFM images. The backbones are oriented in roughly the vertical direction. The patterning was formed by multiple, high-load 1×1 μm^2 scans within the patterned region. The black arrow indicates a bilayer island that has grown in size after the patterning. (c) Far-field fluorescence microscope image of the same region. Characteristic red PCDA fluorescence is localized within the patterned region.

Fig. 12. (a) 1.5×1.5 μm^2 topographic AFM image at the boundary of a tip-induced red PCDA domain. The significant corrugation is aligned along the backbone direction (arrow), and corresponds to bilayer 'valleys' and possibly bilayer 'bumps'. At the bottom of the 'valleys' an oriented PCDA monolayer remains, as seen from the high-resolution 200×200 nm^2 image where the typical backbone striations are observed. (b) Sketch of the observed molecular rearrangement, where bilayer strands have been displaced and relocated on top of the original trilayer.

Fig. 13. Proposed configurations of red (dashed lines) and blue (solid lines) components after the transition. (a) Layers 2 and 3 are removed, and layer 1 is transformed to the red state. (b) Red-phase bilayer strands with shorter backbone lengths (not depicted) are produced. (c) Shear forces convert molecules to the red form and, independently, rearrange some of them.

Fig. 14. Schematic diagram of the molecular orbitals in the π-conjugated PCDA backbone in the planar configuration. Energy levels are affected by the overlap of these orbitals. This overlap would clearly be affected by rotation about one of the C—C backbone bonds. The red phase may consist of a non-planar backbone configuration in conjunction with rotated and/or distorted alkyl side chains, such as a staggered configuration of the side chains.

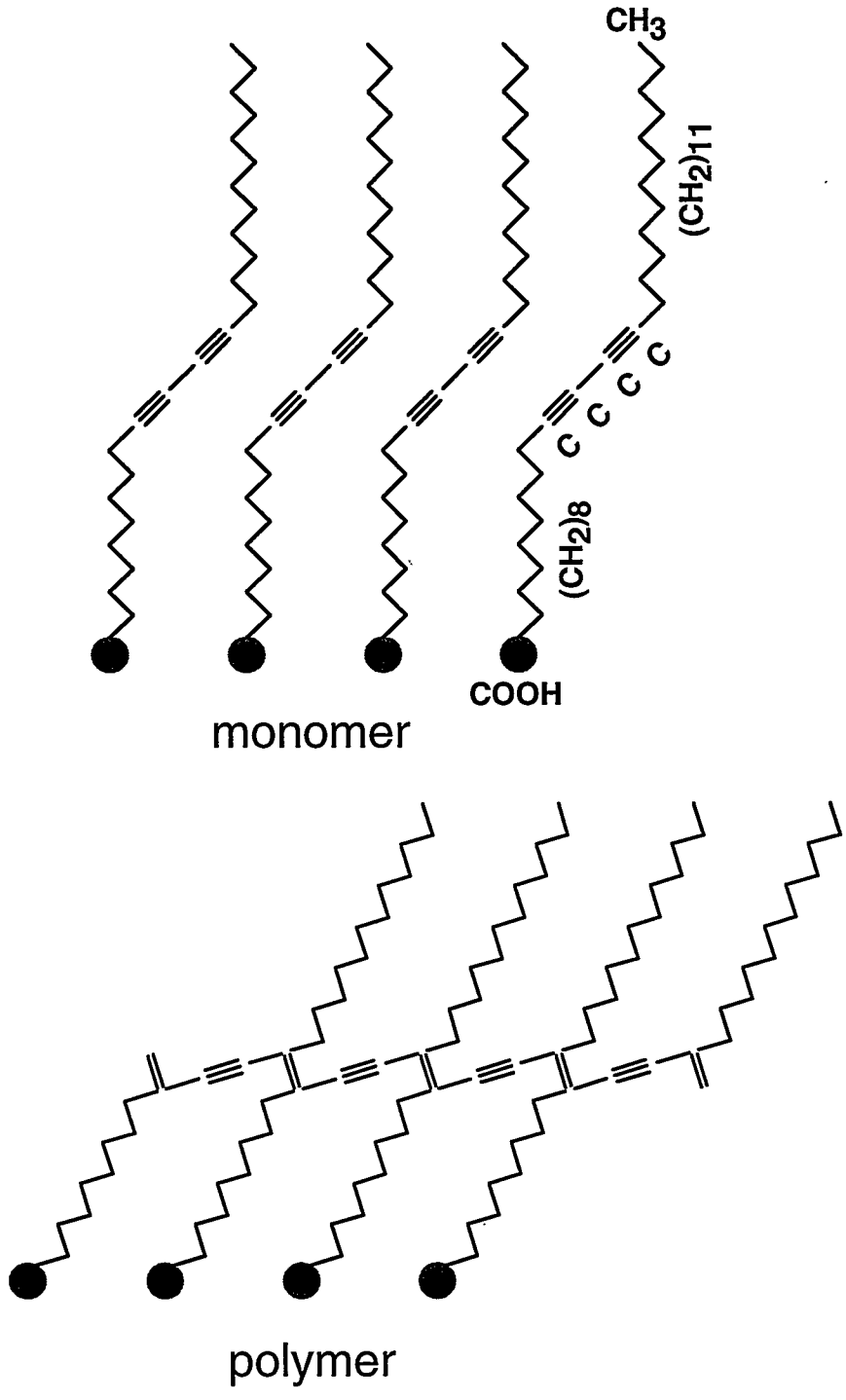

Figure 1

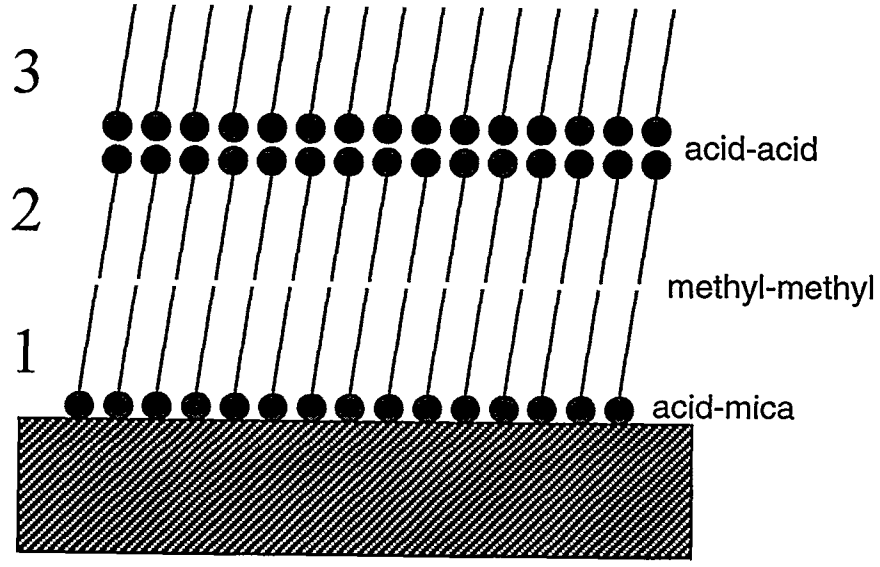

Figure 2

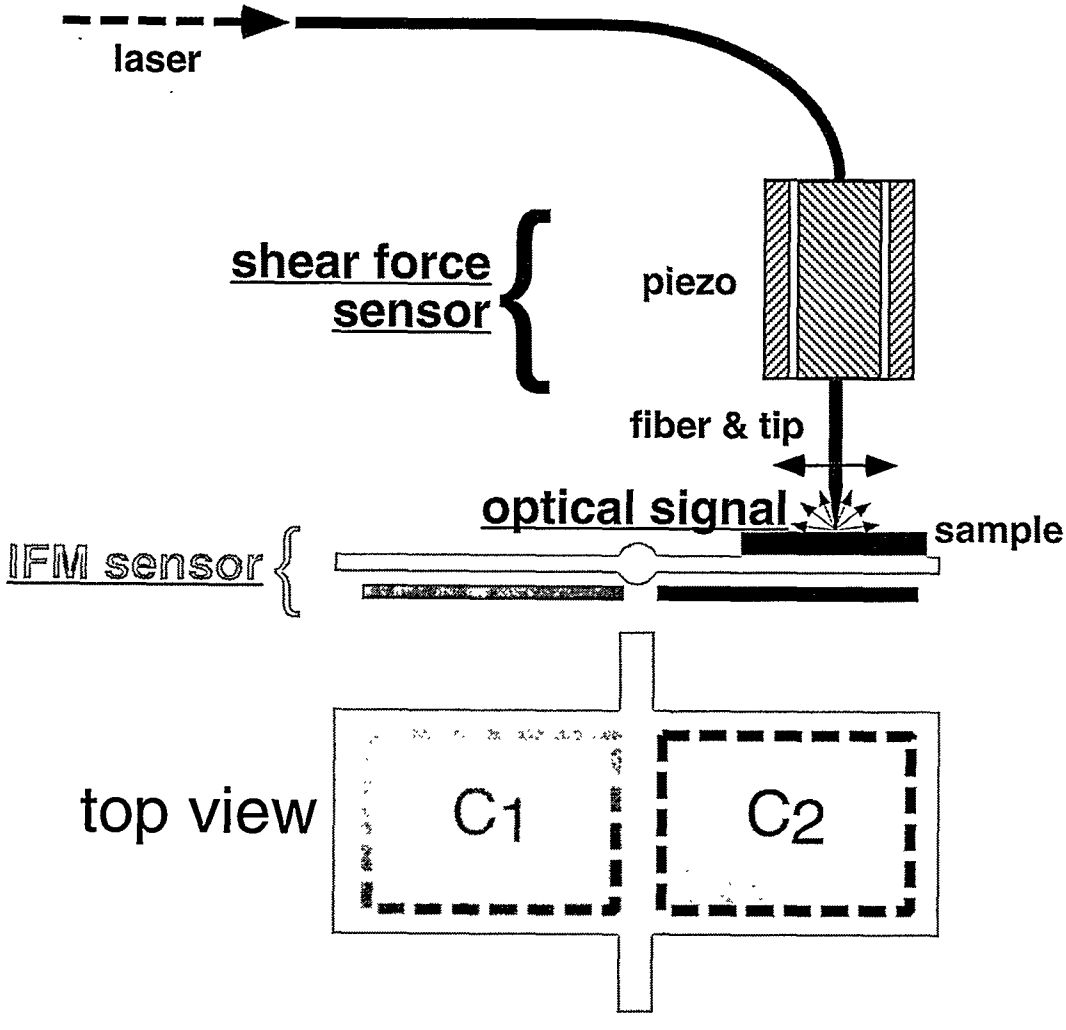
laser
shear force sensor
piezo
fiber & tip
optical signal
sample
IFM sensor
top view
C1
C2

Figure 3

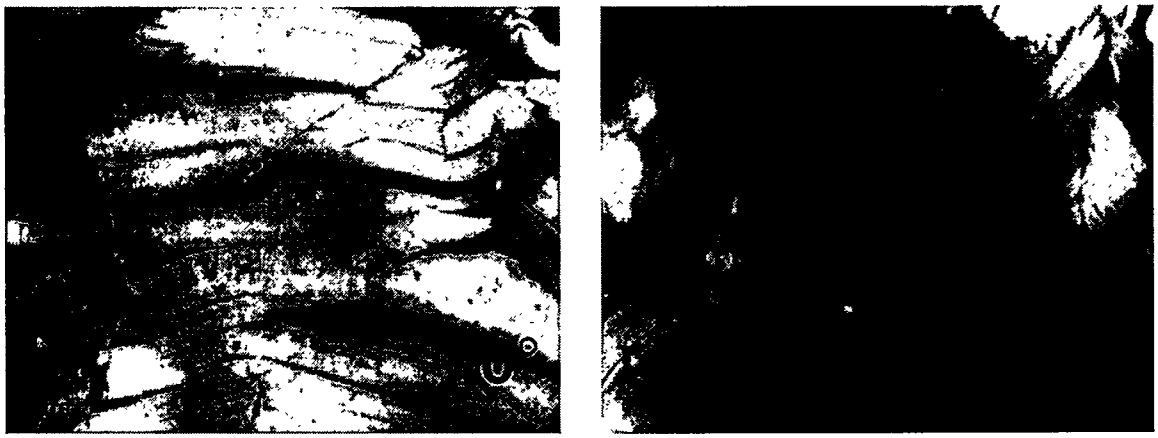

Figure 4

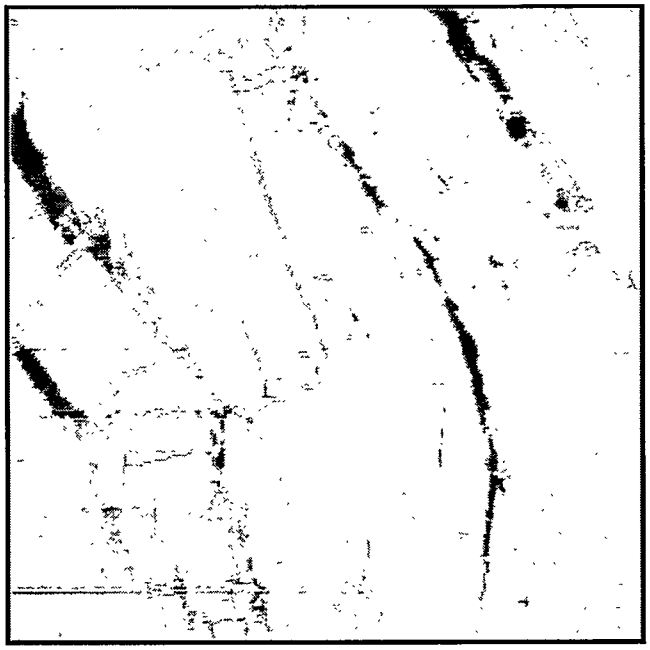

Figure 5

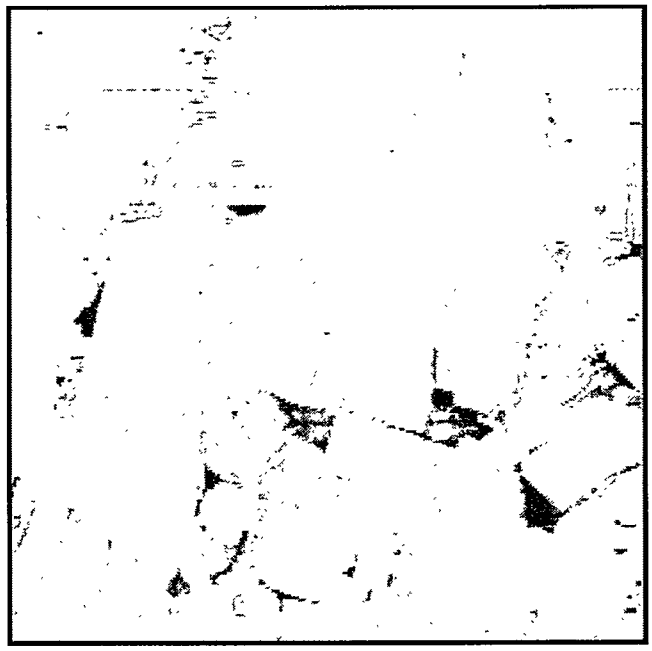

Figure 6

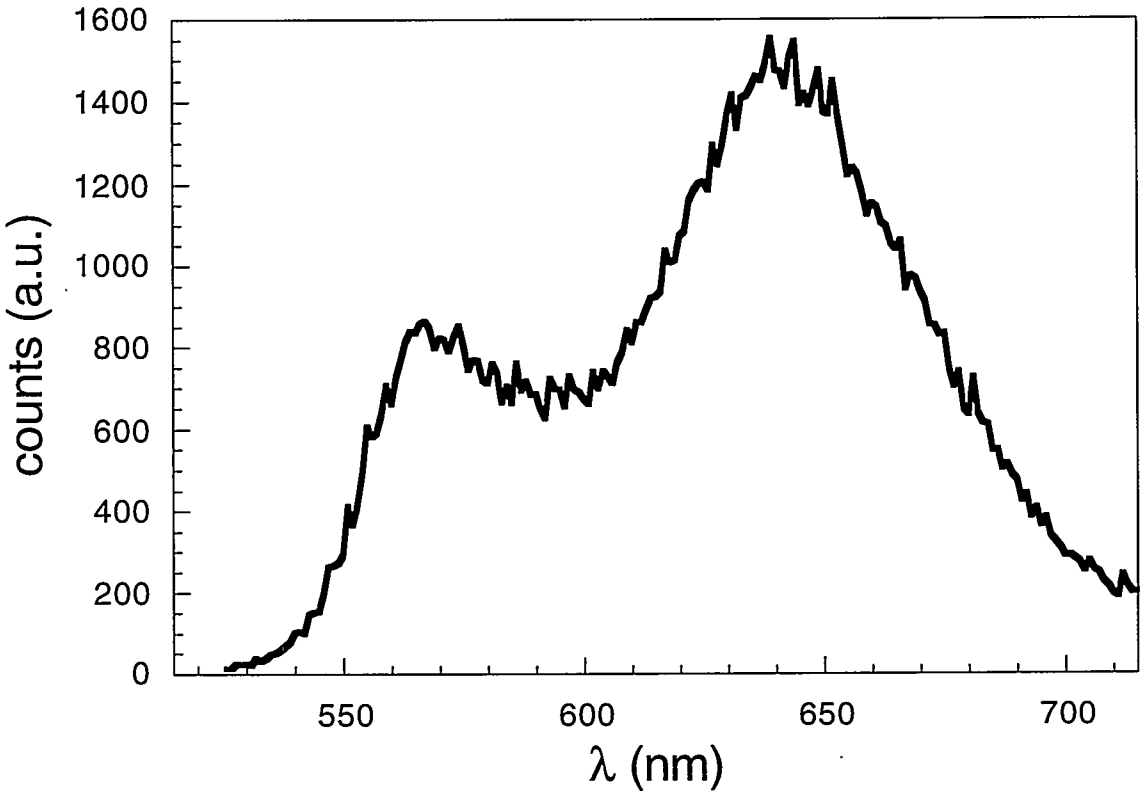
1600
1400
1200
1000
800
600
400
200
0
counts (a.u.)
550
600
650
700
λ (nm)

Figure 7

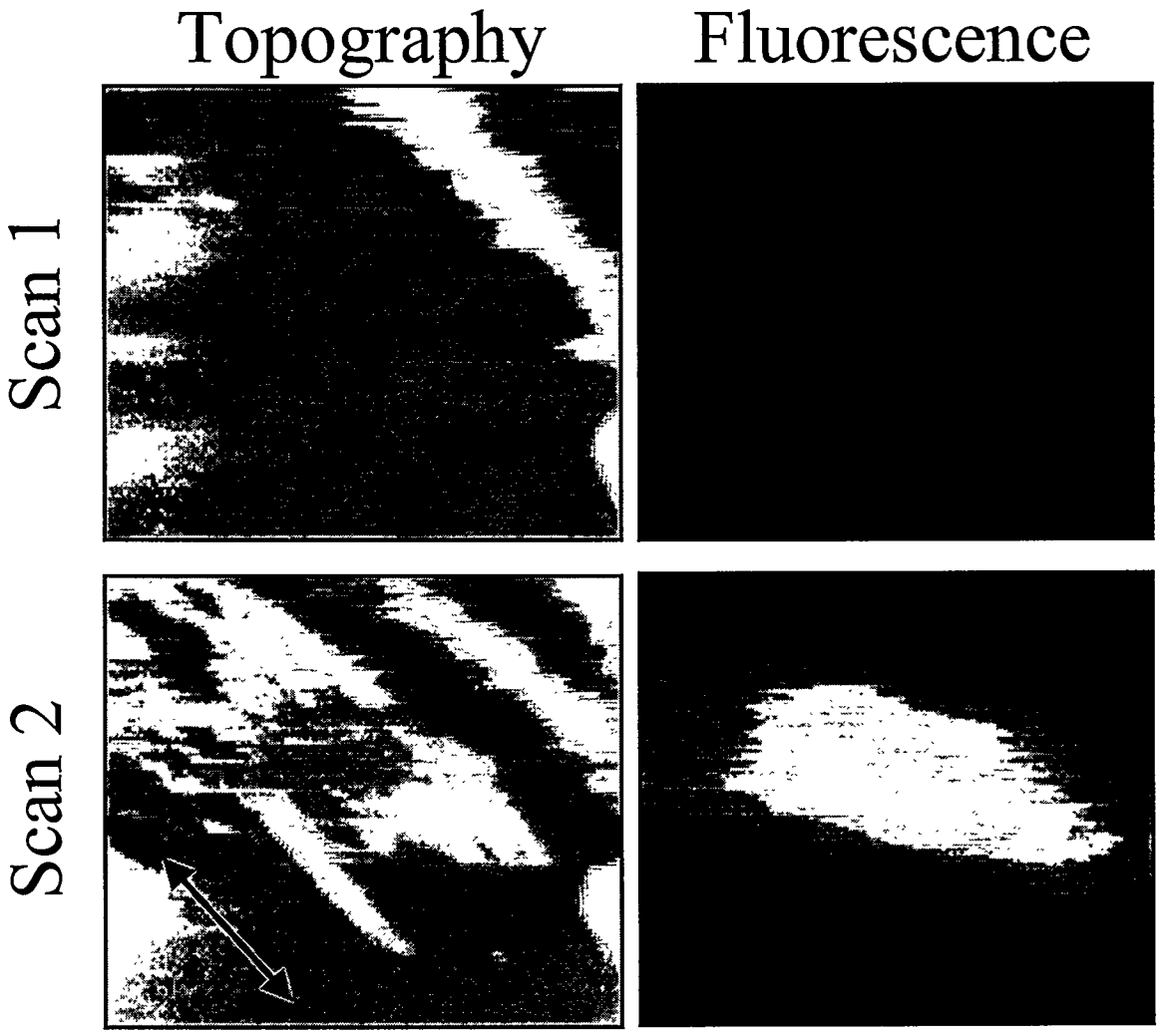

Figure 8

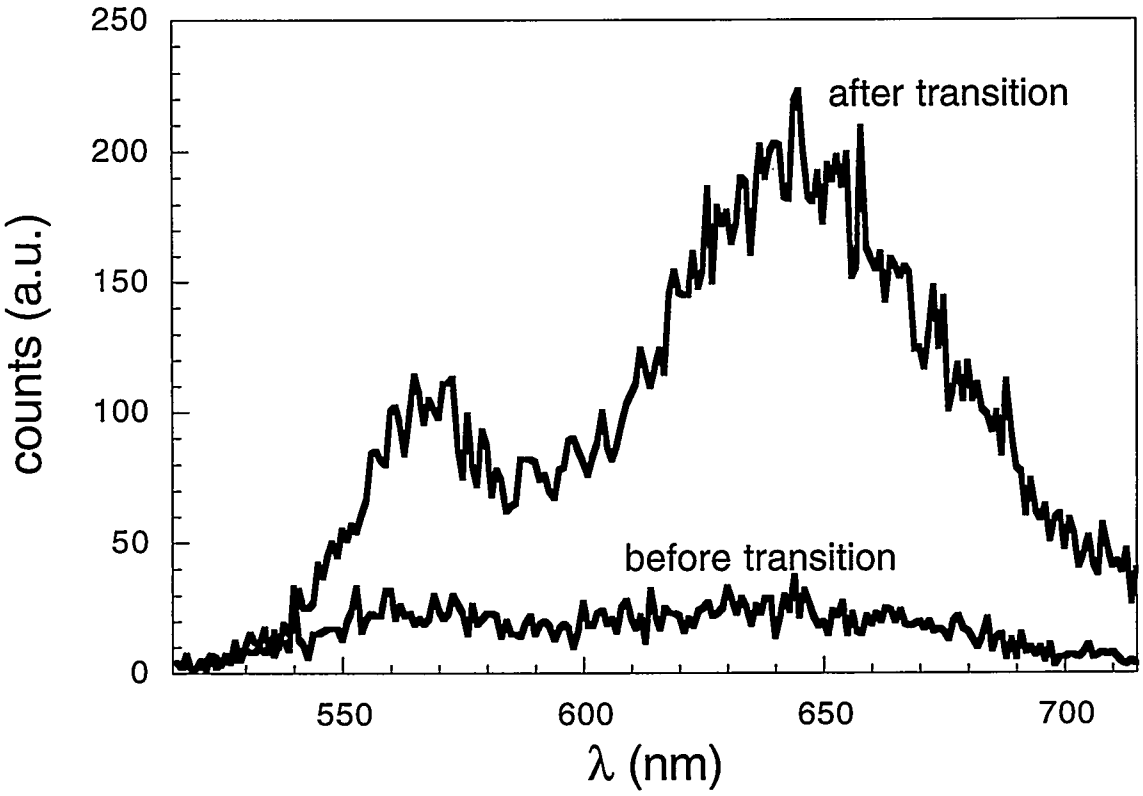
250
200
150
100
50
0
counts (a.u.)
after transition
before transition
550
600
650
700
λ (nm)

Figure 9

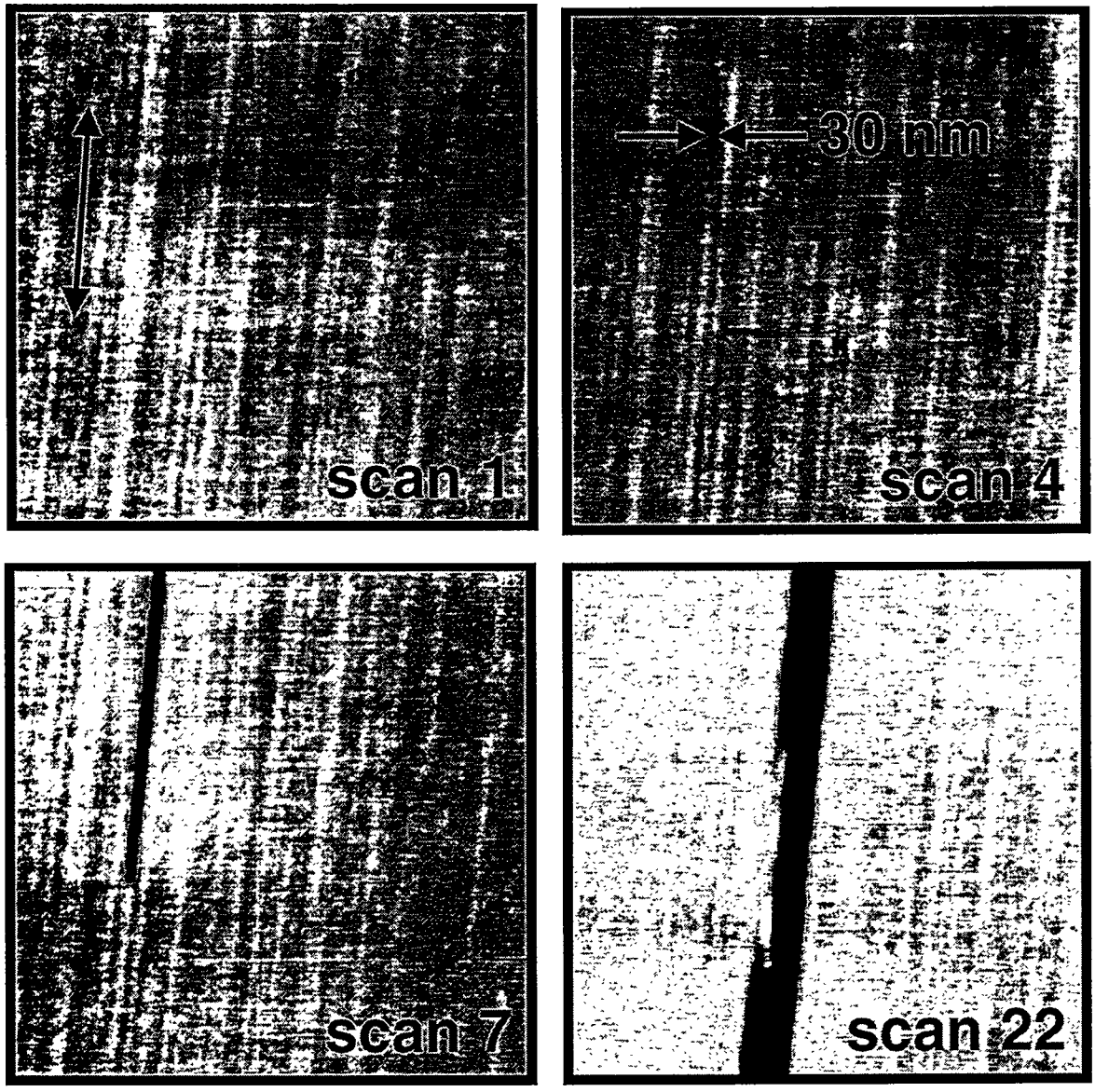

Figure 10

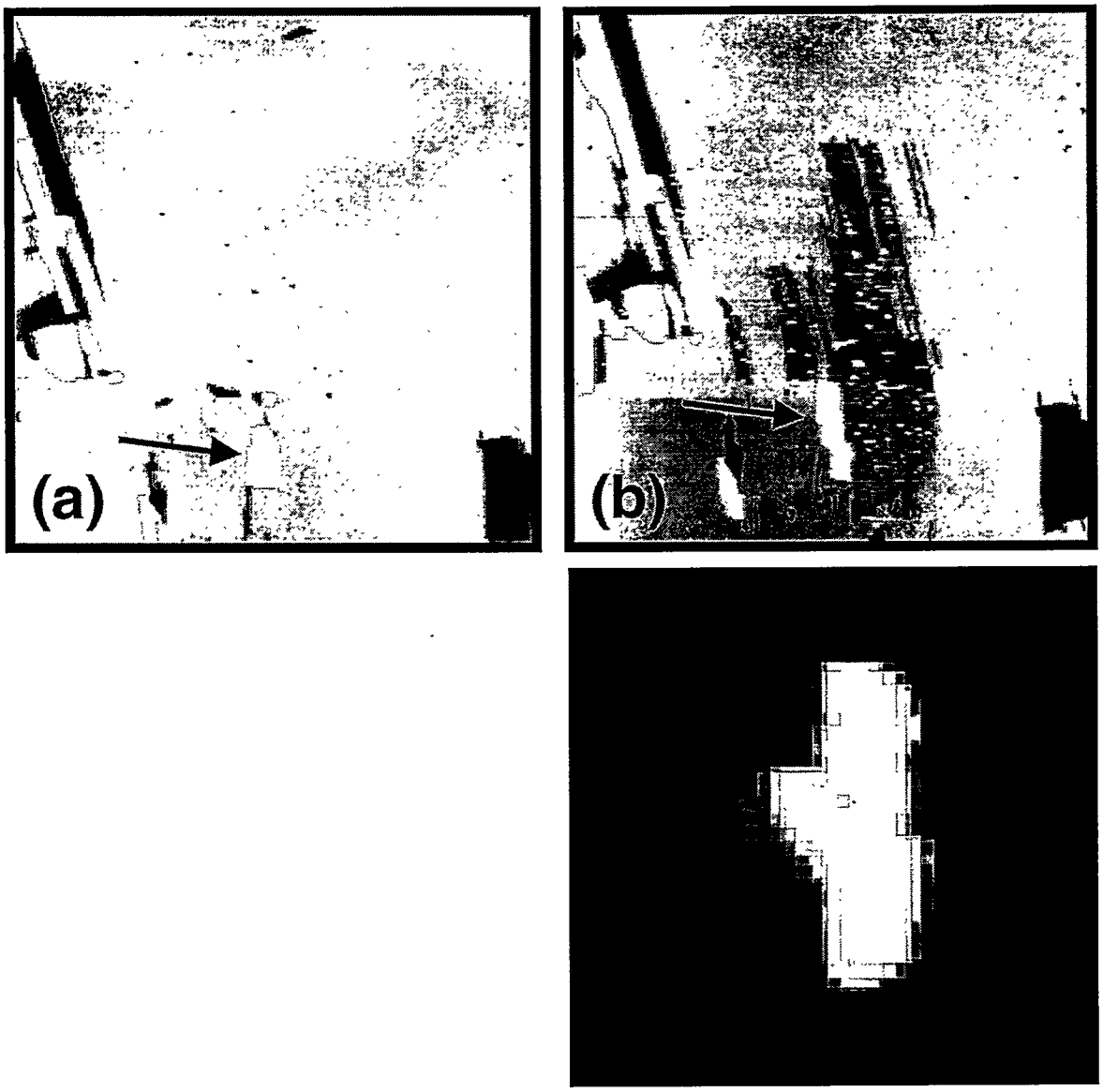

Figure 11

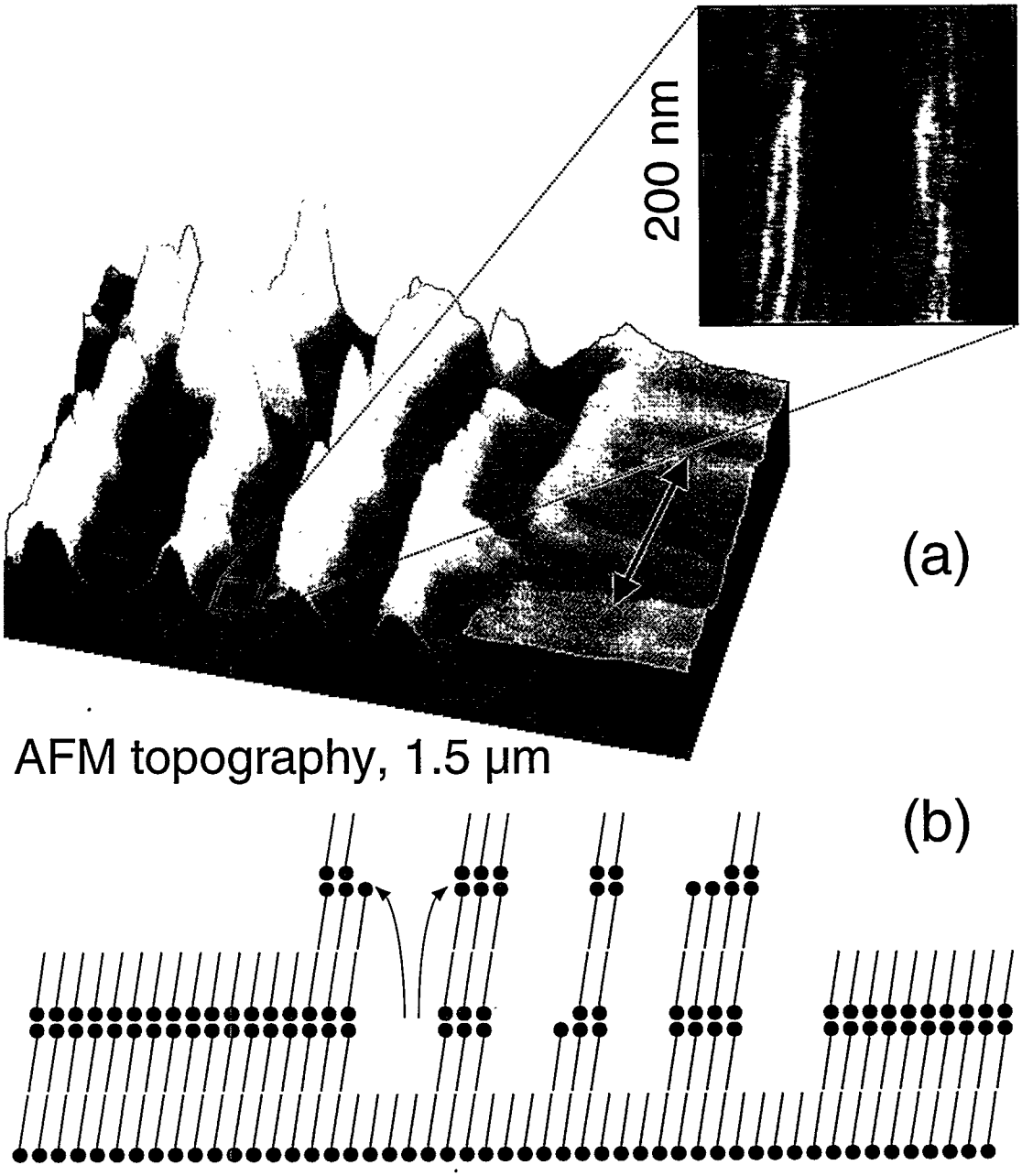

Figure 12

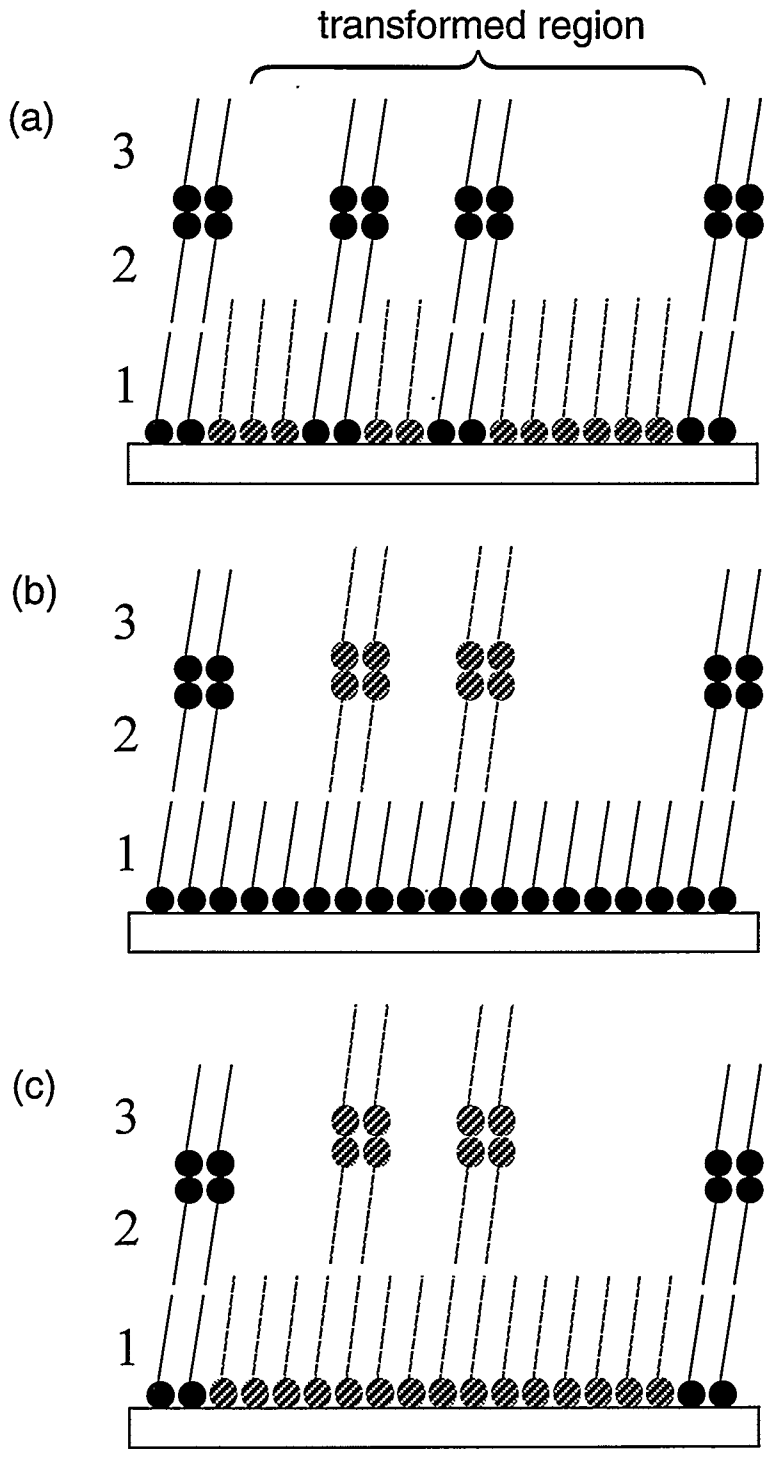

Figure 13

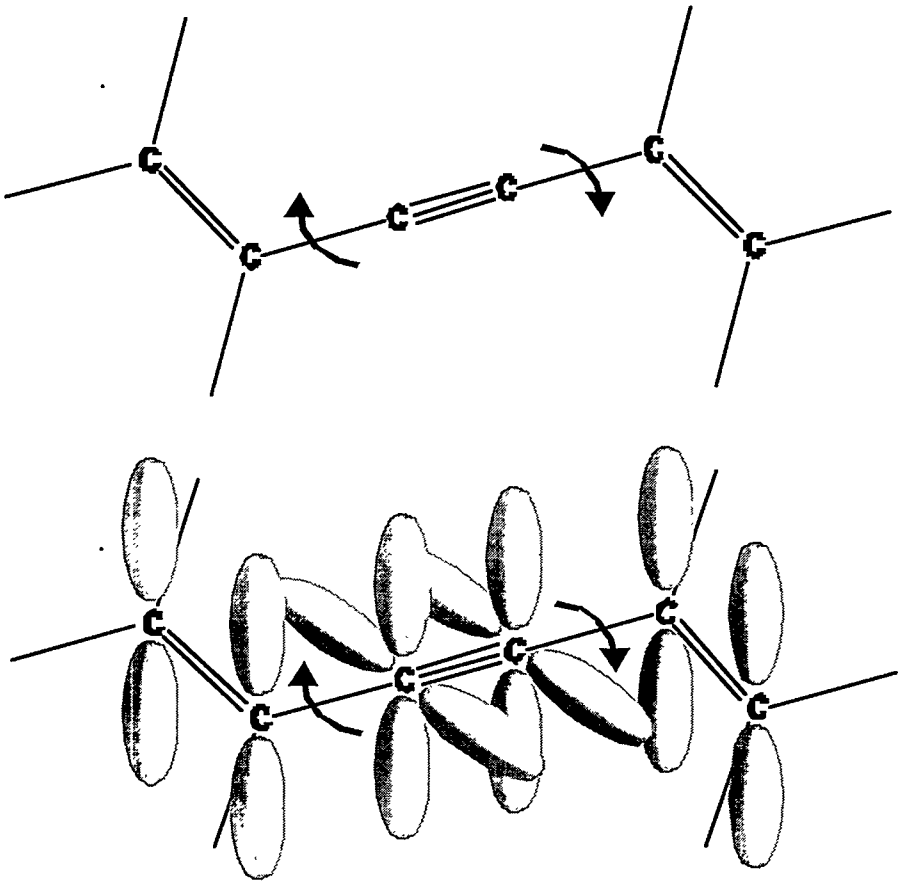

Figure 14